**Seventh International Conference on Computational Fluid Dynamics (ICCFD7), Big Island, Hawaii, July 9-13, 2012**

ICCFD7-1205

# Domain decomposition vs. overset Chimera grid approaches for coupling CFD and CAA

Juliette Ryan*, Laurence Halpern** & Michel Borrel*
Corresponding author: ryan@onera.fr

* ONERA, BP72 - 29 avenue de la Division Leclerc, FR-92322, CHATILLON CEDEX
** LAGA, Université Paris XIII, 99 avenue J.B. Clément, 93430 Villetaneuse, FRANCE .

**Abstract:** This study is a sequel of previous studies done by the authors on coupling CFD and CAA ([1] - [2]). In this paper is recalled the Discontinuous Galerkin method used with the coupling techniques and some new developments are presented. Results are presented for 2D laminar configurations such as a subsonic flow around a cylinder and a mixing layer.

*Keywords:* Euler-Navier Stokes Coupling, Aeroacoustics, Discontinuous Galerkin Method, Time-Space Domain Decomposition.

## 1 Introduction

Computations of aerodynamic sound generation can be classified into different strategies according to the extent of the CFD computational domain, where the Navier-Stokes equations are discretized, and the method used for computing the acoustics [6]. Most CAA computations rely on an acoustic analogy and the so-called Kirchhoff surface surrounding the main acoustic sources to predict the far field. The linear theory inevitably breaks down when flow structures leave the computational domain. At one end of the strategies, the CFD computational domain includes only the near-field region where the main acoustic sources are located. At the other end, the CFD computational domain includes both the near-field and a large part of the acoustic field. For subsonic flows [4], some difficulties can arise with this last strategy due to the large extend of the CFD domain, the small energy level of the acoustic field and the precision of the numerical scheme or of the artificial computational boundary treatment.

In [1] the authors investigated a strategy based on Euler/Navier-Stokes couplings using Schwarz waveform relaxation methods. This strategy relies on a MPI-based parallel domain decomposition method in which the Navier-Stokes equations are discretized only for the near-field and the Euler equations elsewhere, each set of equations runs with its own specific time-space discetization which, for the Euler domain, means sufficient discretization to catch the acoustic scales. The two computations (Navier-Stokes and Euler) can run independently, except at some 'rendez-vous' point in time where data between the different domains are exchanged. For sake of simplicity, a Runge-kutta Discontinuous Galerkin formulation is used [3].

In the present paper, we compare closely the previous domain decomposition approach [2], with the overset Chimera grid approach in which the CAA computational domain extends over the whole computational domain and so can be meshed with an uniform Cartesian grid. In this case, the embedded CFD computational domain is meshed independently according to the scales which have to be taken into account; in the overlaid CAA-region, the nonlinear Euler equations in perturbation are discretized [5], the viscous effects being wrapped up in the source term through a defect-like formulation. In that region, the acoustics are computed twice, firstly in the CFD domain and secondly in the CAA domain: the reason being that some numerical schemes can be good with CFD such as LES but can provide comparatively poor acoustics. Even if we use the same high order scheme like Discontinuous Galerkin in both domains, the limiters needed for the CFD computations deteriorate the pressure waves. Special attention is paid to the multi-scale aspect requiring highly non conforming space-time discretization for which the discontinuous Galerkin approach is particularly well adapted.

For this study, both the near-field and the far-field have to be computed together, so, as many grid configurations have to be tested and in order to have less computational effort, only two-dimensional flows at low Reynolds numbers will be considered such as the sound emitted by the flow around a cylinder and by vortex pairing in a perturbed mixing layer.

# 2 Numerical Discretization

## 2.1 Governing equations

The governing equations to be solved are the Euler and the Navier-Stokes equations in 2D for a compressible flow which express conservation of mass, momentum and energy

$$\partial_t \mathcal{W} \ + \ \nabla \cdot \mathbf{F}(\mathcal{W}) - \ \nabla \cdot \mathbf{F}^D(\mathcal{W}, \nabla \mathcal{W}) = \mathbf{0} \tag{1}$$

where $\mathcal{W} \ = \ (\rho, \ \rho\overrightarrow{\mathrm{U}}, \ \rho \mathrm{E})$ is the conservation variable vector with classical notations, $\mathbf{F}$ represents the Euler fluxes:

$$\mathbf{F} \ = \ \Big(\rho\overrightarrow{\mathrm{U}} \ , \ \rho\overrightarrow{\mathrm{U}} \otimes \overrightarrow{\mathrm{U}} \ + \ pI \ , \ \overrightarrow{\mathrm{U}} \ ( \ \rho E \ + \ p \ ) \Big) \tag{2}$$

and $\mathbf{F}^D$ represents the diffusion and heat fluxes of the Navier-Stokes equations:

$$\mathbf{F}^D \ = \ \Big( 0 \ , \ \overline{\overline{\tau}} \ , \ \overline{\overline{\tau}} \cdot \overrightarrow{U} + \lambda \nabla T \Big) \, . \tag{3}$$

Above $\rho$ is the density, $\overrightarrow{U} = (u, v)$ the velocity, $\overline{\overline{\tau}}$ the shear stress tensor, $p$ the pressure, $T$ the temperature, $E = e + (u^2 + v^2)/2$ the total energy with $e$ the specific internal energy and $\lambda$ is the thermal conductivity. We assume the gas to be calorically perfect, with the heat capacities $c_v, c_p$ and the Prandtl number constant ($Pr = 0.72$). So, we can express $e = c_v T$ and $\lambda = c_p \mu / Pr$ where $\mu$ is the dynamic viscous coefficient taken constant or given by Sutherland's law. The pressure $p$ is given with the perfect polytropic gas state law $p = \rho R T = (\gamma - 1) \rho e$ with $R = c_p - c_v$ the specific gas constant and $\gamma$ the specific heat ratio ($\gamma = c_p / c_v = 1.4$). The Newtonian fluid hypothesis and the Stokes relation define the shear stress tensor in terms of the dynamic viscosity coefficient $\mu$ and the gradient of the velocity:

$$\overline{\overline{\tau}} \ = \ \mu \ \left( \nabla \overrightarrow{U} + (\nabla \overrightarrow{U})^T - \frac{2}{3} (\nabla \cdot \overrightarrow{U}) \overline{\overline{I}} \right) . \tag{4}$$

## 2.2 DG formulation

The Euler or the Navier-Stokes equations are solved in a domain $\Omega$ discretized by either a Cartesian or an unstructured triangular grid $\mathcal{T}_h = \bigcup \Omega_i$ and the associated function space $V_h$

$$V_h = \{ \phi \in L^2(\Omega) \mid \phi / \Omega_i \in P_k \} \tag{5}$$

where $P_k$ is the space of polynomials of degree k.

The DG formulation based on a weak formulation after a first integration by parts is of the form : find $\mathcal{W}^h$ in $(V_h)^4$ such that for all $\Omega_i$ in $\mathcal{T}_h$ ,

$$\forall \phi \in V_h, \quad \int_{\Omega_i} \partial_t \mathcal{W}_h \ \phi \ dx = \int_{\Gamma_i} (\mathbf{F}_h - \mathbf{F}_h^D) \ \phi \ d\gamma - \int_{\Omega_i} (\mathbf{F}_h - \mathbf{F}_h^D) \nabla \phi \ dx. \tag{6}$$

Here, the numerical fluxes $\mathbf{F}_h$,$\mathbf{F}_h^D$ and $\mathcal{W}_h$ are approximations of $\mathbf{F}$, $\mathbf{F}^D$ and $\mathcal{W}$ . The Euler fluxes $\mathbf{F}$ are classically determined using the LLF (Local Lax-Friedrichs) or HLLC fluxes ([8]); we will detail in the next section the viscous flux computation through the EDG method.

If we neglect locally the dependency of $\mu$ on temperature, the viscous term $\mathbf{F}^D$ can be split into a linear and a nonlinear part,

$$\mathbf{F}^D = \mathcal{L}(\nabla\overrightarrow{U}, \nabla T) + \mathcal{N}(\overrightarrow{U}\cdot\tau). \tag{7}$$

A second integration by parts can be done on the linear part $\mathcal{L}(\nabla\overrightarrow{U}, \nabla T)$ thus giving the following formulation,

$$\begin{aligned}\forall\phi\in V_h,\quad \int_{\Omega_i}\partial_t\mathcal{W}_h\;\phi\;dx = \;& \int_{\Gamma_i}(\mathbf{F}_h - \mathbf{F}_h^D + \mathcal{L}(\overrightarrow{U}, T))\;\phi\;d\gamma \\ & -\int_{\Omega_i}(\mathbf{F}_h + \mathcal{L}(\overrightarrow{U}, T) - \mathcal{N}(\overrightarrow{U}\cdot\tau))\nabla\phi\;dx.\end{aligned} \tag{8}$$

Finally, we take in the space $V_h$ a basis built locally with the Legendre polynomials, this basis being orthogonalized for triangle elements. So, this formulation results in a system of coupled ordinary differential equations of the form

$$\mathcal{M}\;\partial_t\mathbf{W}_h = \mathbf{R}(\mathbf{W}_h) \tag{9}$$

where $\mathbf{W}_h$ is the vector containing the degrees of freedom (DOF) associated to $\mathcal{W}_h$ expressed in a basis of $V_h$ and $\mathcal{M}$ the mass matrix, which is diagonal, while $\mathbf{R}$ are the residuals which are nonlinear functions of $\mathbf{W_h}$. We have chosen the explicit time stepping RK3 of Shu-Osher [9] to solve (Eq. 9). As usual, the time step is subject to a CFL-like restriction.

## 2.3 The EDG method

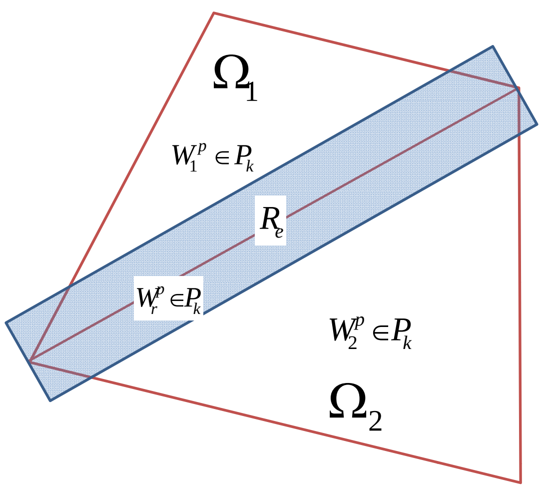


Figure 1: Definition of the elastoplast element (color area) overlapping the interface between two triangular elements $\Omega_1$, $\Omega_2$. .

We are only concerned here with the diffusion terms. The simple idea of the EDG method is to regularize locally the discontinuous solution $\mathcal{W}_h$ over each edge using an $L^2$ projection in a rectangular interpolation element $E$ overlapping this edge (see Fig. 1). The basis in $E$ of the same order k as the DG basis defined in the elements, using on either side of the edge an equal number of Gauss quadrature points, which number provides at least the order of the original solution.

More precisely, for any interface $\Gamma$ between elements $\Omega_1$ and $\Omega_2$, the regularized solution in $E$ is expanded in the DG-$P_k$ basis:

$$\mathcal{W}_E = \sum_p W_E^p \phi_E^p \tag{10}$$

where $\phi_E^p$ represents the DG-$P_k$ basis functions and $W_E^p$ the unknowns which are computed by:

$$W_E^p = \frac{1}{(\phi_E^p, \phi_E^p)_E}\left(\int_{\Omega_1\bigcap E} W_1^p\phi_E^p dx + \int_{\Omega_2\bigcap E} W_2^p\phi_E^p dx\right). \tag{11}$$

Above, $W_1^p$ and $W_2^p$ are the local DG-$P_k$ solutions in $\Omega_1$ and $\Omega_2$, $(\bullet,\bullet)_E$ is the $L^2$ product in $E$,

$$\forall \phi, \psi \in L^2(\Omega)\ (\phi,\psi)_E = \int_E \phi\psi dx \tag{12}$$

All integrals are numerically computed using a n-point Gaussian quadrature rule with n defined such that $2*n-1 \geq k$, where k is the order of polynomials of the DG formulation.

Once the $L^2$ projection is done, each conservation variable has a polynomial expression in the elastoplasts E. Following the Cauchy-Kovalewsky procedure (cf. [10]), it is possible to introduce in E a space-time approximation by expressing all time derivatives via spatial derivatives:

$$\begin{cases} \partial_t \mathcal{W} \ = - \dfrac{\partial \mathbf{F}}{\partial \mathcal{W}} \ \cdot \ \nabla \mathcal{W} \\[2ex] \partial_t \nabla \mathcal{W} \ = - \dfrac{\partial^2 \mathbf{F}}{\partial \mathcal{W}^2} \ \cdot \ (\nabla \mathcal{W})^2 \ - \ \dfrac{\partial \mathbf{F}}{\partial \mathcal{W}} \ \cdot \ \nabla(\ \nabla \mathcal{W}) \\[2ex] \partial_{tt} \mathcal{W} \ = - \dfrac{\partial^2 \mathbf{F}}{\partial \mathcal{W}^2} \ \cdot \ (\partial_t \mathcal{W})(\nabla \mathcal{W}) \ - \ \dfrac{\partial \mathbf{F}}{\partial \mathcal{W}} \ \cdot \ \partial_t \ \nabla \mathcal{W}. \end{cases} \tag{13}$$

and so on, the needed quantities being computed 'au fur et a mesure'. Above, $\mathbf{F}$ stands both for the Euler and the Navier-Stokes fluxes. In practice, the calculations are carried out componentwise. This space-time approximation allows us to update the data in the elastoplasts only at the beginning of each time step and not at each RK sub-iteration, the fluxes being updated using a time Taylor expansion.

As in [1],this idea of the elastoplast interpolation at the inter-elements is generalized to the Euler/Navier-Stokes coupling.

# 3 Euler/Navier-Stokes Couplings

## 3.1 Domain decomposition coupling

### 3.1.1 Schwarz waveform relaxation methods

These methods are based on Schwarz domain decomposition algorithms, invented by H.A. Schwarz in 1870 [11]. In order to solve a Laplace equation in the domain $\Omega$, it is split into two subdomains with overlap $\Omega_1$ and $\Omega_2$, in which the equation is solved alternatively. Exchange of information is made on the boundaries by exchange of Dirichlet values. This algorithm has been extended by P.L. Lions to nonoverlapping subdomains using different transmission conditions, such as Robin conditions [19]. For an extension to evolution problem, we couple it to a waveform relaxation algorithm, which is an extension both of the Picard's "approximations successives" and relaxation methods for algebraic systems, due to Lelarasmee [18]. Versions with Dirichlet or optimized Robin transmission conditions have been designed in [12] for the unsteady heat equation with prescribed Dirichlet boundary conditions and initial data:

$$\begin{cases} \partial_t u \ - \ \nu \ \triangle u \ = f & \text{in } \Omega \times [0,T] \\ u(x,0) \ = \ u_0(x) & \text{in } \Omega \\ u \ = \ g & \text{on } \partial\Omega \end{cases} \tag{14}$$

where $u$ is the temperature, $\nu$ is the constant diffusive coefficient and $\triangle$ represents the Laplace operator. A parallel version of the Schwarz waveform relaxation algorithm can be generalized from a decomposition in two domains $\Omega = \Omega_1 \cup \Omega_2$ associated with two spatial operators $\mathcal{L}_1$ and $\mathcal{L}_2$, and two interface operators $\mathcal{B}_1$ and $\mathcal{B}_2$ (called the transmission conditions) as

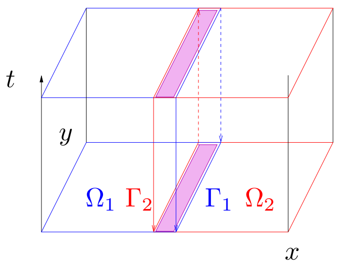


$$\begin{cases} \partial_t u_1^k - \mathcal{L}_1 u_1^k = f & \text{in } \Omega_1 \times (0,T), \\ u_1^k(\cdot,0) = u_0 & \text{in } \Omega_1, \\ \mathcal{B}_1 u_1^k = \mathcal{B}_1 u_2^{k-1} & \text{on } \Gamma_1 \times (0,T), \\ u_1^k = g & \text{on } (\partial\Omega_1 - \Gamma_1) \times (0,T), \end{cases}$$

$$\begin{cases} \partial_t u_2^k - \mathcal{L}_2 u_2^k = f & \text{in } \Omega_2 \times (0,T), \\ u_2^k(\cdot,0) = u_0 & \text{in } \Omega_2, \\ \mathcal{B}_2 u_2^k = \mathcal{B}_2 u_1^k & \text{on } \Gamma_2 \times (0,T), \\ u_2^k = g & \text{on } (\partial\Omega_2 - \Gamma_2) \times (0,T). \end{cases}$$

If we take for the transmission operators $\mathcal{B}_j = Id$, an overlap between the domains is necessary. Optimal transmission conditions (Robin conditions) can be written for the heat equation as

$$\mathcal{B}_j = \nu \partial_{n_j} + p \ \ , \ j = 1, 2 \tag{15}$$

where $n_j$ is the unit normal exterior to $\Gamma_j$. The relaxation parameter $p$ is determined asymptotically as a function of the physical parameters, the size of the space-time domains and the mesh parameters (see [12]). In that case we can use adjacent domains without overlap.

We have in [1] extended this algorithm for systems and more precisely by taking for operators $\mathcal{L}_1$ and $\mathcal{L}_2$ the Navier-Stokes and the Euler operators respectively. The Dirichlet or the Robin conditions at the interface will be applied in through an integral formulation computed with the relevant Gauss nodes. Notice that $\nu = 0$ for the Euler operator and that $\nu$ is no longer a constant for the Navier-Stokes operator.

#### 3.1.2 Implementation

General technique: to compute Euler fluxes (resp. viscous fluxes) at interface boundaries, 3 gauss point values are needed on the interface (resp. 9 gauss point values in the EDG cell). All necessary DOF are sent to the other domain asynchronously so that fluxes can be computed in a transparent way, whether there are rectangular or triangular elements.

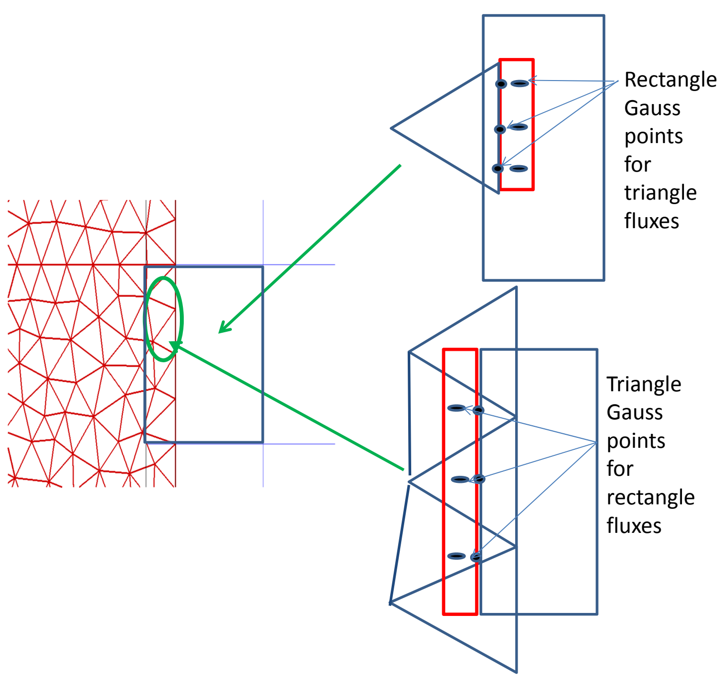


Figure 2: Definition of the coupling in space.

We have to couple the Schwarz sub-iterations (parameter $k$ in the equations above) with the time stepping (RK3) used in the domains $\Omega_1$ and $\Omega_2$, but with different time steps. We want to use a parallel algorithm. Time windows are defined in such a way that time coincides on the two domains at the end of the time window for both domains. Then the local CFL number is adjusted so that m time steps are performed in domain $\Omega_1$ and n time steps are performed in domain $\Omega_2$ within each time window. Fig. 3 shows an example of a whole Schwarz iteration in a time window defined at the interface between two domains $D_1$, $D_2$. Here, the dots represent the DOF, the vertical arrows represent the full time steps, the horizontal red lines represents the $j^{th}$ RK iterations and the horizontal arrows represent the exchange data for the parallel computing. The Gauss DOF, which are to be interpolated at Gauss integration nodes in the domain $D_2$, are only represented for the domain $D_1$. Notice that the blue and yellow Gauss DOF are interpolated in time separately.

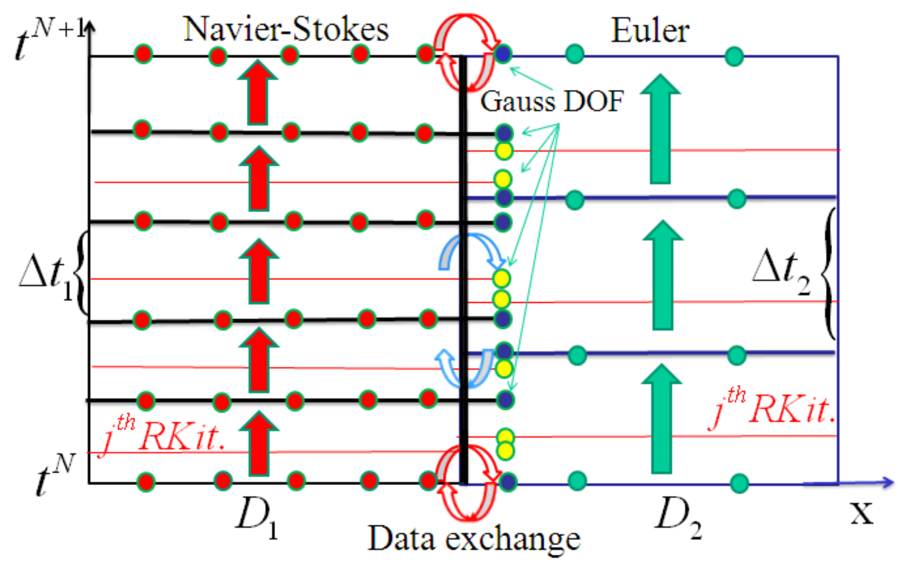


Figure 3: Definition of the coupling in time.

Sketch of one Schwarz iteration in a time window defined at the interface between two domains $D_1$, $D_2$. Here, the dots represent the DOF, the vertical arrows represent the full time steps, the horizontal red lines represents the $j^{th}$ RK iterations and the horizontal arrows represent the exchange data for the parallel computing. The Gauss DOF, which are to be interpolated at Gauss integration nodes in the domain $D_2$, are only represented for the domain $D_1$. Notice that the blue and yellow Gauss DOF are interpolated in time separately.

Domains proceed in time independently, using at first predefined interface values. At the end of the time window, domains exchange their newly computed boundary cells values for all time steps (including sub times for the Runge Kutta scheme) and a new time march is carried out with updated interface values. This iterative procedure is repeated till solution ceases to vary. This method allows for different time steps and different space interface discretization as received values from other domains can be interpolated and projected on the local time-space grid.

In time, when enough time steps exist per window, different quadratic interpolations are used to interpolate the DOF in the ghost element. Asynchronous exchange data are performed inside the time window with few impact on the parallel computing time.

Notice that a non iterative algorithm could perhaps be devised as in [21] using an ADER procedure, but as two or three iterations are generally sufficient to converge we take benefit of a very general and simple algorithm.

## 3.2 Hierarchical overset Chimera grid coupling

### 3.2.1 Euler equations in perturbation

If we consider the acoustics as a linear perturbation of the mean flow of the CFD flow field, the governing equations of the CAA are the linearized Euler equations. An important issue of the coupling between the CFD and the CAA is then to define the mean flow. In fact, as we want to limit the CFD domain as much as possible, the coupling area (where Navier-Stokes and Euler are both defined) is located in a zone where the nonlinear effects are very important and the linearized Euler equations are no more relevant within a fully coupled approach. In that context, the Euler equations in perturbation open the door to an other interesting possibility to a full Navier-Stokes computation.

Here, two overlapping domains are considered $G_{NS}$ and $G_{CAA}$ with $G_{NS}$ completely embedded in $G_{CAA}$. On $G_{NS}$ is computed a Navier-Stokes solution $\mathcal{W}_{NS}$.

$$\partial_t \mathcal{W}_{NS} \ + \ \nabla \cdot \mathbf{F}(\mathcal{W}_{NS}) - \ \nabla \cdot \mathbf{F}^D(\mathcal{W}_{NS}, \nabla \mathcal{W}_{NS}) = \mathbf{0} \tag{16}$$

with the same notations as in (Eq. 1).

On $G_{CAA}$, the following decomposition is used : $\mathcal{W} = \mathcal{W}_0 + \mathcal{W}'$ where $\mathcal{W}$ satisfies the Navier-Stokes equations :

$$\partial_t \mathcal{W} \ + \ \nabla \cdot \mathbf{F}(\mathcal{W}) - \ \nabla \cdot \mathbf{F}^D(\mathcal{W}, \nabla \mathcal{W}) = \mathbf{0} \tag{17}$$

and $\mathcal{W}_0$ is defined by the assumption that all viscous effects are described with $\mathcal{W}_0$, that is :

$$\nabla \cdot \mathbf{F}^D(\mathcal{W}, \nabla \mathcal{W}) = \nabla \cdot \mathbf{F}^D(\mathcal{W}_0, \nabla \mathcal{W}_0) \tag{18}$$

Thus the Euler equations in perturbation can be written:

$$\partial_t \mathcal{W}' \ + \ \nabla \cdot \mathbf{F}(\mathcal{W}) = -(\partial_t \mathcal{W}_0 \ - \ \nabla \cdot \mathbf{F}^D(\mathcal{W}_0, \nabla \mathcal{W}_0) = RHS(t) \tag{19}$$

Let $P$ be the projection operator of the instantaneous values defined on $G_{NS}$ onto $G_{CAA}$. $\mathcal{W}_0$ is approximated by $P(\mathcal{W}_{NS})$. Two approximations based on (Eq. 16) of the right hand side $RHS(t)$ can be made

$$RHS(t) \quad = \quad \nabla \cdot \mathbf{F}(P(\mathcal{W}_{NS})) \tag{20}$$
$$RHS(t) \quad = \quad P(\nabla \cdot \mathbf{F}(\mathcal{W}_{NS}) \tag{21}$$

### 3.2.2 Implementation

The implementation of this coupling is very close to the AMR techniques. One time step consists in two stages:

1. The Navier-Stokes solution $\mathcal{W}_{NS}$ is computed on $G_{NS}$ and projected onto $G_{CAA}$ providing $\mathcal{W}_0$ and the right hand side for (Eq. 19).

2. The Euler equations in perturbation are then computed on $G_{CAA}$ providing new boundary conditions for the Navier-Stokes problem on $G_{NS}$.

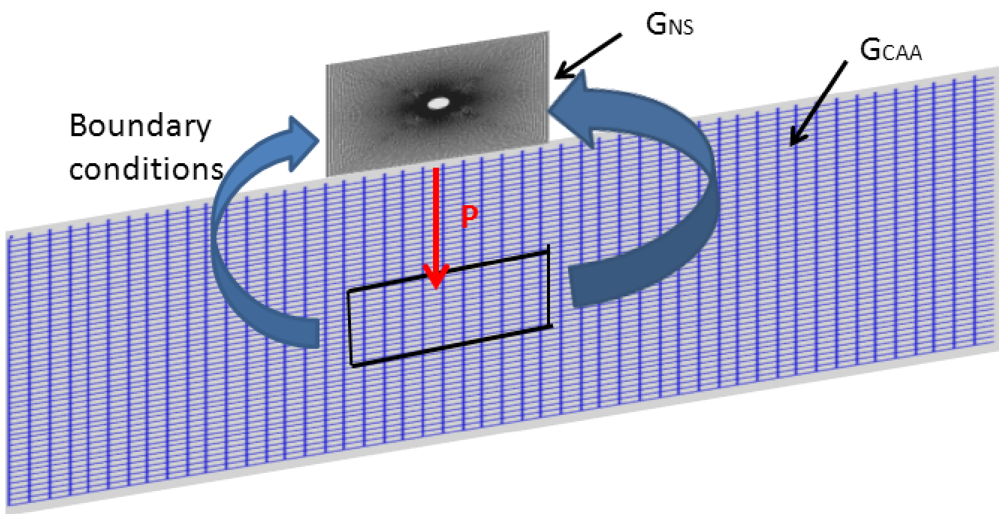


Figure 4: Chimera overlapping grids

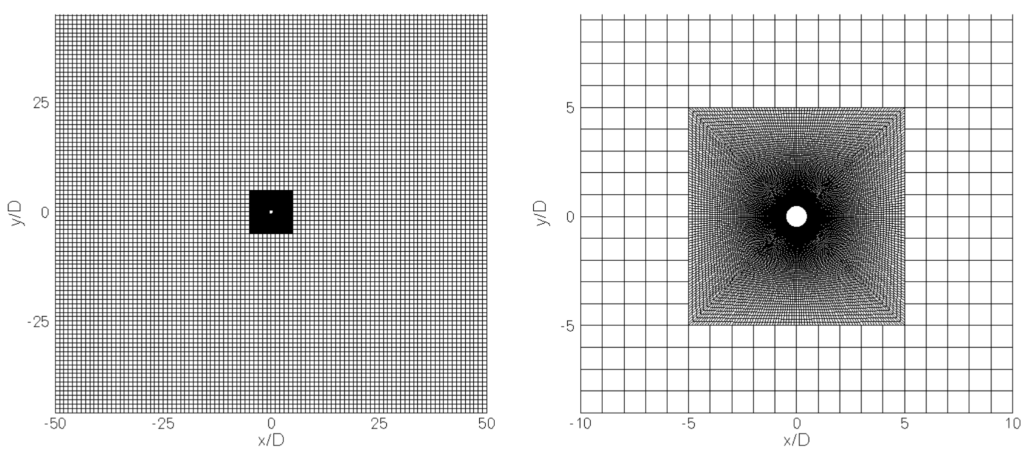


(a) Global Mesh

(b) Zoom

Figure 5: Chimera mesh seen from above

# 4 DDM versus Chimera

In our parallel context associated to the explicit time scheme, surrounding Euler domains (where the studied acoustics waves reside) get their boundary values from the Chimera/Navier-Stokes domain from interpolated (L2 projection) values on the EDG cell. For either approach (DDM or Chimera), these values will be the same if the chimera domain is identical to the underlying domain and more accurate in the case of DDM if more refined as there will be less interpolations.
For the Chimera/Navier-Stokes domain, it gets its boundary values from the Euler surrounding domains again with an EDG technique. The main difference between the two methods is the additional underlying Euler with perturbation domain in the case of the chimera approach.

# 5 Numerical Results

All computations are DG-$P_2$, no limiters were used for either Euler or Navier-Stokes computations. For both Cartesian and unstructured computations, we used the same functional space $V_h$. The triangular grid used has been obtained with the freeware mesh generator Gmsh [20]. In the following computations, all adjacent computational domains slightly overlap over 10

## 5.1 Laminar flow around a cylinder at low-Reynolds number

This academic 2D test case is that of the flow around a cylinder [13]-[14]. A low Reynolds number based on the diameter $Re_D = \rho_\infty u_\infty D/\mu_\infty = 500$ is chosen in order to remain below the onset of 3D behavior, and not to have to use limiters. The upstream Mach number is $M_\infty = 0.33$ and we fix the cylinder diameter $D = 1$, the freestream density is $\rho_\infty = 1$ and velocity is $u_\infty = 1$. On outside boundaries are imposed non reflecting boundary conditions.

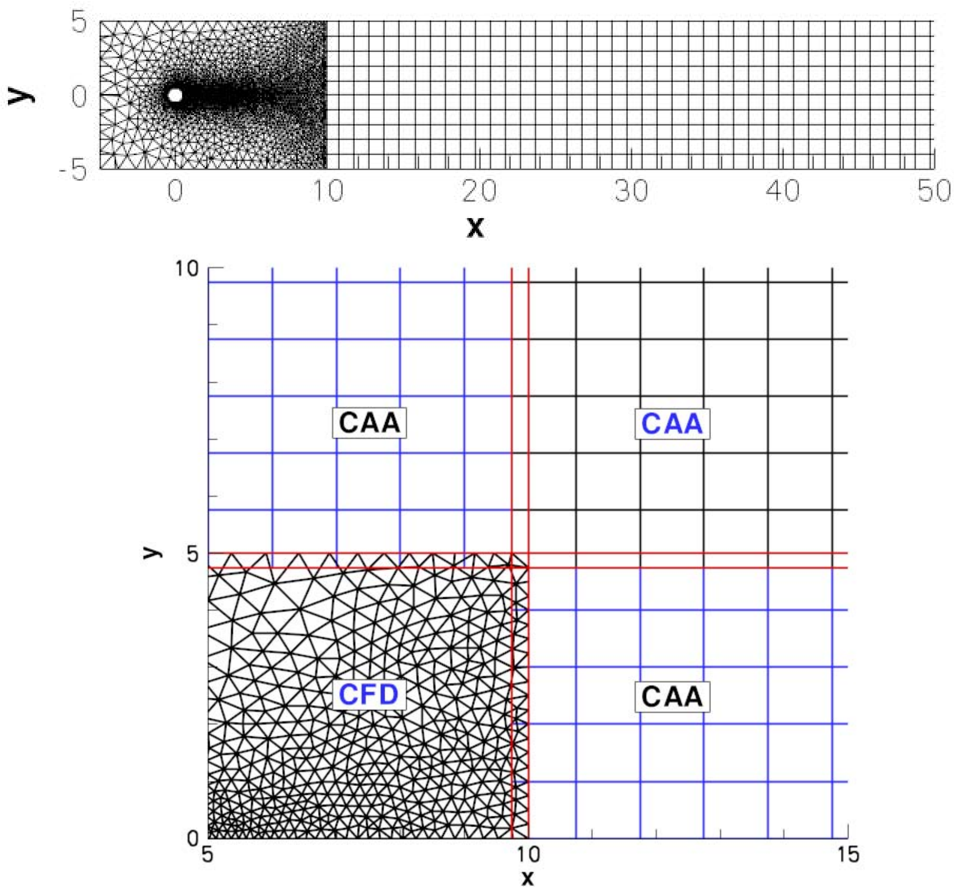


Figure 6: Cylinder: enlarged views of the composite mesh in the near-field vortex shedding region (up) and about a CFD/CAA coupling boundary (down). In red is the overlapping zone.

All the space dimensions are scaled with the cylinder diameter D. The composite mesh consists of an unstructured CFD mesh near the cylinder and a Cartesian uniform CAA mesh with a mesh spacing of 1 (Figure 6). The CFD domain extends arbitrarily $10D$ downwards and the CAA domain extends from $-150D$ to $300D$. The unstructured mesh around the cylinder consists of 14000 triangles with 62 triangles along the cylinder and 40 triangles at the boundary $x = 10$ (Figure 6-down). In order to suppress spurious reflections of the acoustic waves at outflow boundaries, a sponge layer zone is introduced all around the physical region(Figure 7).

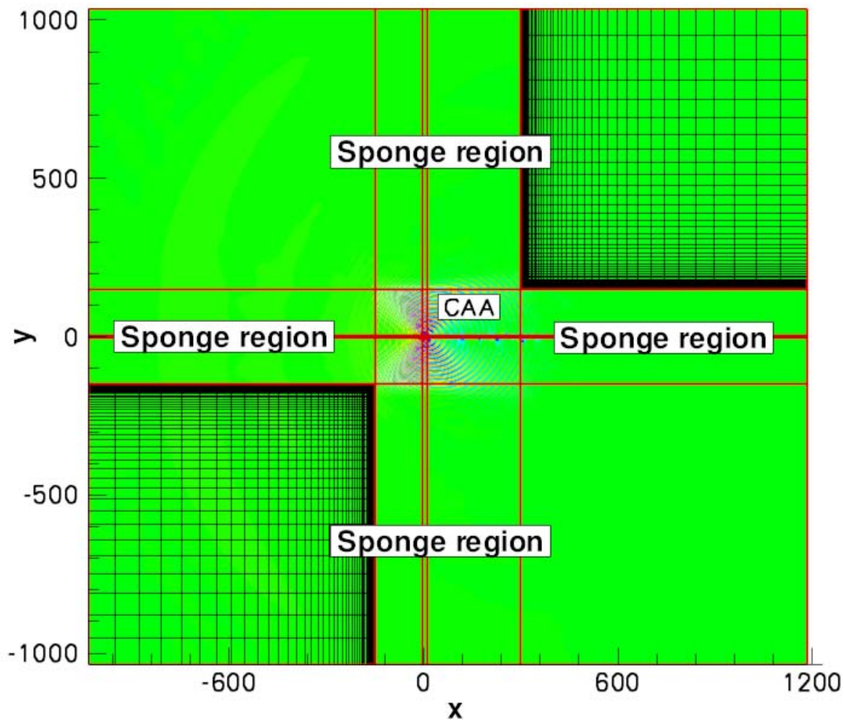


Figure 7: Cylinder configuration: the 25 computational sub-domains with instantaneous acoustic pressure field.

The simulations are performed until time $t = 300$. This is sufficient to establish completely vortex shedding and propagation of the acoustics to the full domain with a statically stationary flow field. Several computations have been made. In all the computations, the Navier-Stokes equations are used in the CFD mesh and the compressible Euler equations are used in the non-overlapped part of the CAA mesh.

The computation has been run with one to two Schwarz sub-iterations for the Euler- Navier-Stokes computation for time windows the size of 10 Navier-stokes time steps and 2 to 3 Euler time steps, which allow us to converge to sixth order for each time window. In the embeddded Navier-Stokes - Euler computation, the Navier-Stokes domain computes 3 time steps against one time step for the Euler domain.

All three computations give similar instantaneous pressure fields and a Strouhal number of .23 .

Figure 8 shows instantaneous vorticity and acoustic pressure defined as $p_{acou} = (0.15246\,p - 1)1e + 5$. Non-dimensioned vorticity color scale is between -1.5 and 1.5 and pressure color scale is between -200 and 200 Pa. This scale allows to emphasis the acoustic modes. As is to be expected, the acoustic radiation is almost dipolar from the cylinder. The Von Karman vortex shedding in the near wake region is well described and further diffused in the CAA domain. No spurious pressure wave reflections or sound sources are visible in the instantaneous acoustic pressure contours.

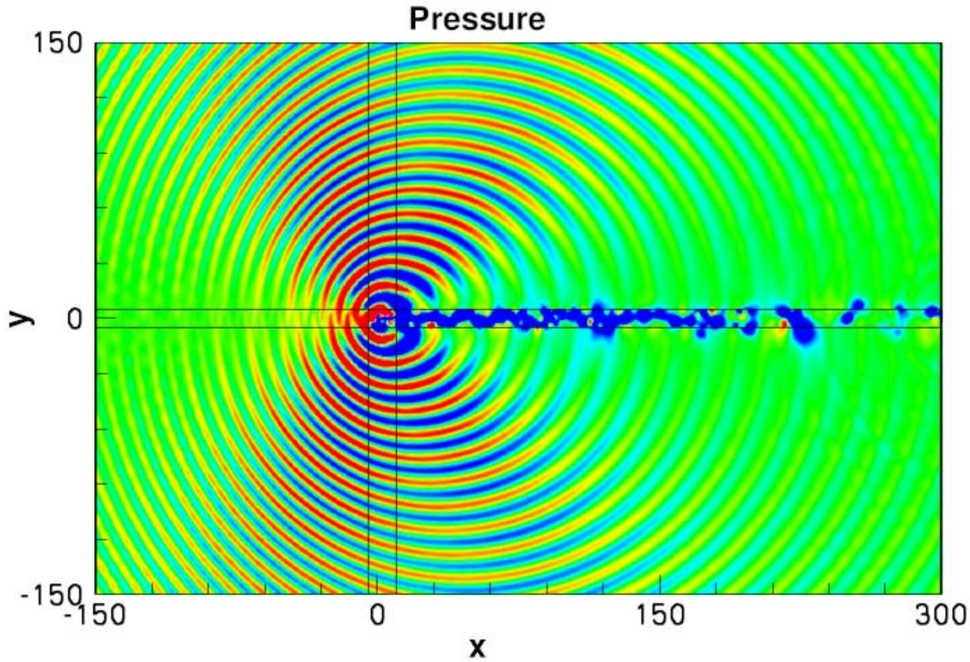


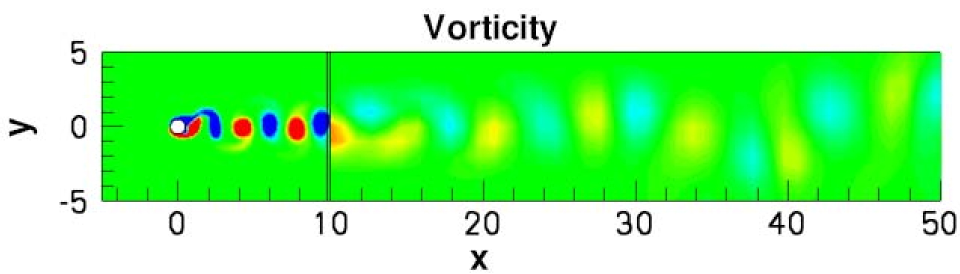


Figure 8: Flow around a cylinder at low Reynolds number: instantaneous acoustic pressure field (up) and vorticity (down).

**Remark on the role of upper and lower sponge layers:** Without upper and lower sponge layers, spurious reflections of pressure waves at the boundaries, due to approximate non reflecting conditions, can lead to a non-physical pressure waves. The apparent origin of these waves is located at the vortex shedding near the downstream boundary according to the symmetry chosen. Introducing a sponge layer only in the downstream direction doesn't suppress the phenomena as we can see in Figure 9.

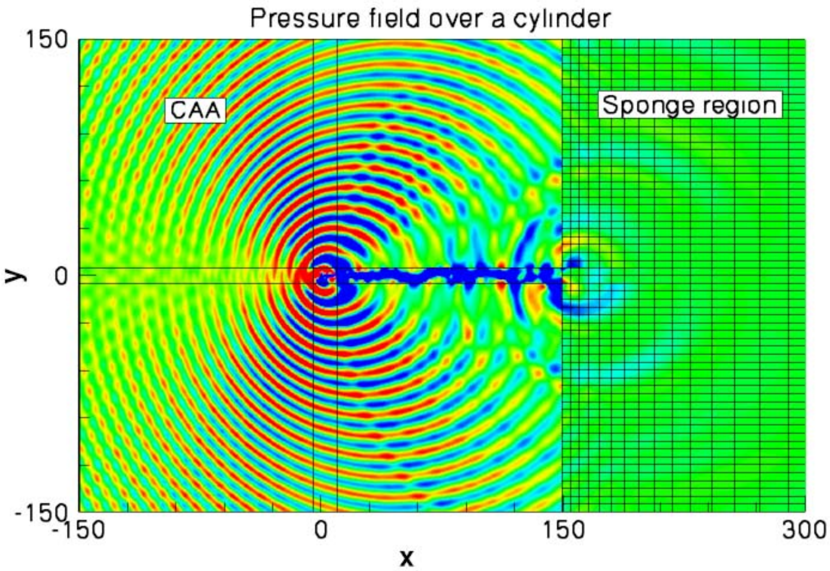


Figure 9: Instantaneous acoustic pressure fields around a cylinder without upper and lower sponge layers.

### 5.2 Sound generation in a 2D mixing layer

This second academic case is chosen to test the proposed methodology on another noise source mechanism associated with flow instabilities in free shear flows. The flow configuration is the same as the one proposed by Colonius, Lele and Moin [4]. It concerns the time-dependent flow of a compressible mixing layer. It has been computed by many authors (see for example [13] with DG computations). As pointed out by Gassner, LÖrcher and Munz [22], this test case is very challenging for a direct simulation of sound generation/propagation specially with DG because the numerical treatments at the artificial boundaries can act as significant source of sound. Authors using finite difference schemes introduce low-pass filtering which are difficult to extend in a straightforward manner to DG.

The upper and lower Mach numbers are $M_\infty = 0.5$ and $M_{-\infty} = 0.25$, respectively. Dimensioning with the sound velocity, the upper and lower x-velocity, density and pressure can take the values $u_\infty = 0.5$, $u_{-\infty} = 0.25$, $\rho_\infty = \rho_{-\infty} = 1$ and $p_\infty = p_{-\infty} = 1/\gamma$, respectively, with $\gamma = 1.4$. An hyperbolic tangential shape velocity profile is define:

$$u = \bar{u} + 0.125\, tanh(2y) \tag{22}$$

with $\bar{u} = (u_\infty + u_{-\infty})/2$. Lengths are normalized with vorticity thickness of the layer at $x = 0$:

$$\delta_\omega = \left. \frac{\Delta u}{(du/dy)_{max}} \right|_{x=0} \tag{23}$$

with $\Delta u = u_\infty - u_{-\infty}$.The Reynolds number $Re = \rho_\infty \Delta u \delta_\omega / \mu$ defined by the velocity jump, vorticity thickness and dynamic viscosity at the free-stream temperature is set to 250. Equal temperature through the mixing layer is assumed and the dynamic viscosity is taken constant.

In order to investigate the sound generated by vortex roll up and pairings, the mixing layer is forced at its most unstable frequencies. Disturbances are added to the initial mean velocity profiles, corresponding to a fundamental frequency $f = \omega_1$ and subharmonic frequencies $f/2$, $f/4$ and $f/8$:

$$\left\{\begin{array}{lcl} u' & = & \sum_{k=1}^{4} a_k \dfrac{y\bar{u}}{\pi\omega_k b} sin(2\pi\omega_k t + \phi_k)\ exp(-y^2/b) \\ v' & = & \sum_{k=1}^{4} a_k cos(2\pi\omega_k t + \phi_k)\ exp(-y^2/b) \end{array}\right. \tag{24}$$

where $b = 5$ is the y-modulation and $a_k$ are the amplitudes of the disturbances. The fundamental frequency $f = \omega_1$ is 0.0501 and the phase shifts $\phi_k, k$ =2,3,4 of the sub-harmonics are: -0.028, 0.141 and 0.391. The amplitudes of the disturbances are $a_1 = 0.0037$, $a_2 = 0.0073$, $a_3 = 0.007$ and $a_4 = 0.0103$. This provide a standard mean divergence-free disturbances to the mixing layer in an efficiently excited mode.

The physical region extends to $0 \leq x \leq 400$ and $-200 \leq y \leq 200$. A sponge layer is added downstream,up and above from x=400 to x=672 and from y=200 (resp. y=-200) to y=1000 (resp. y=-100)(see Figure 10) meshed with a stretched coarse grid (20 grid nodes) along the each direction. Euler equations are solved everywhere except in the near-field mixing region which extends to $0 \leq x \leq 400$ and $-10 \leq y \leq 10$ where the Navier-Stokes equations are solved. The location of the upper and lower boundary has been placed intentionally too close with respect of the mixing layer boundary in order to test the present coupling method.

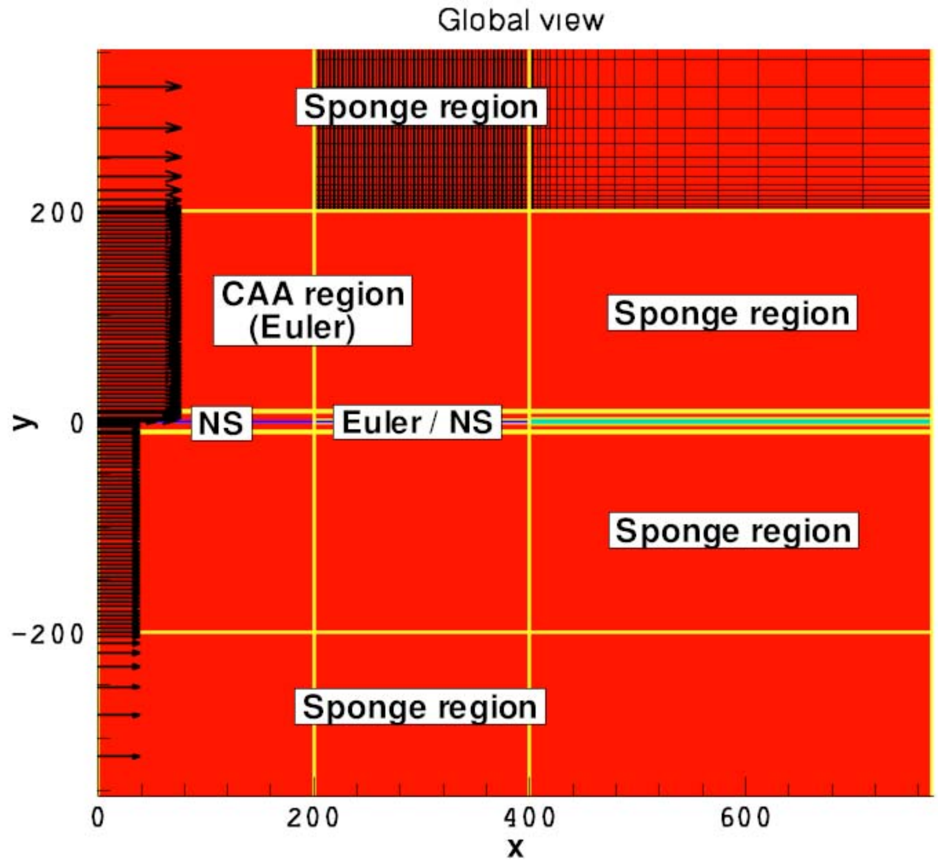


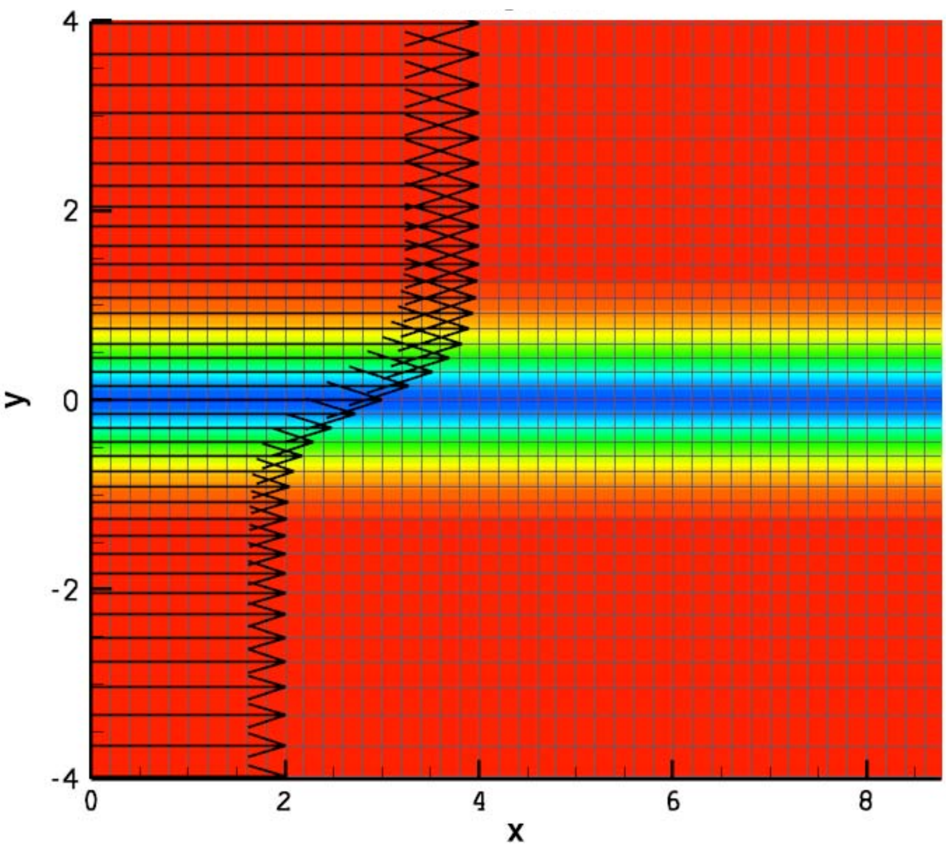


Figure 10: Mixing layer configuration: the 15 computational sub-domains with initial velocity, global view (up) and enlarged view (down).

The CAA domain is meshed with a uniform Cartesian grid and a grid meshing of 1. The NS computational domain is meshed using a 1001 x 61 Cartesian grid built as in [3], with equally spaced nodes in the x-direction and stretched in the y-direction, using the mapping

$$y \;=\; \frac{L_y}{2}\frac{sinh(b_y\eta)}{sinh(b_y)} \tag{25}$$

where the length in the y direction is $L_y = 20$ and the stretching factor $b_y = 2.4$. The equally spaced mapped coordinate $\eta$ runs from -1 to +1. This corresponds to a smooth stretching in the normal direction with a grid spacing of $\Delta y = 0.15$, $\Delta x = 0.2$ in a region round $y = 0$ so that about 12 grid points are inside the initial mixing layer (see Figure 11).

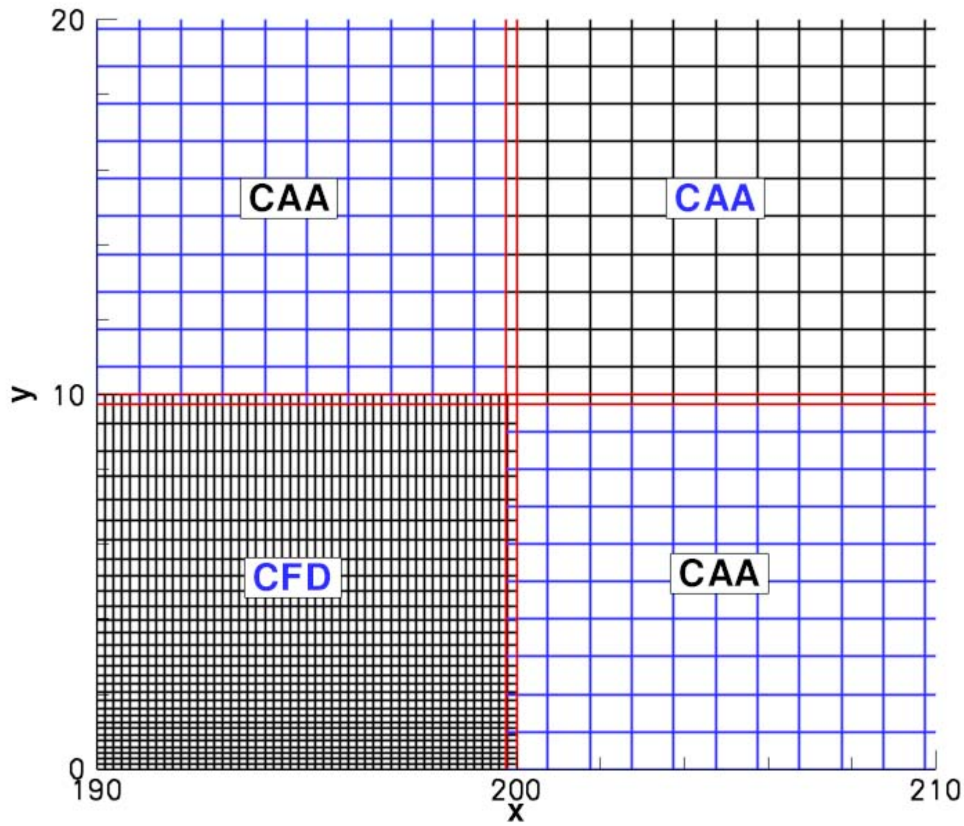


Figure 11: Mixing layer: enlarged view of the composite mesh near CFD/CAA coupling boundary. In red is the overlapping zone.

Non reflecting conditions are imposed on the upper and lower boundaries and on the downstream boundaries of the sponge domains.

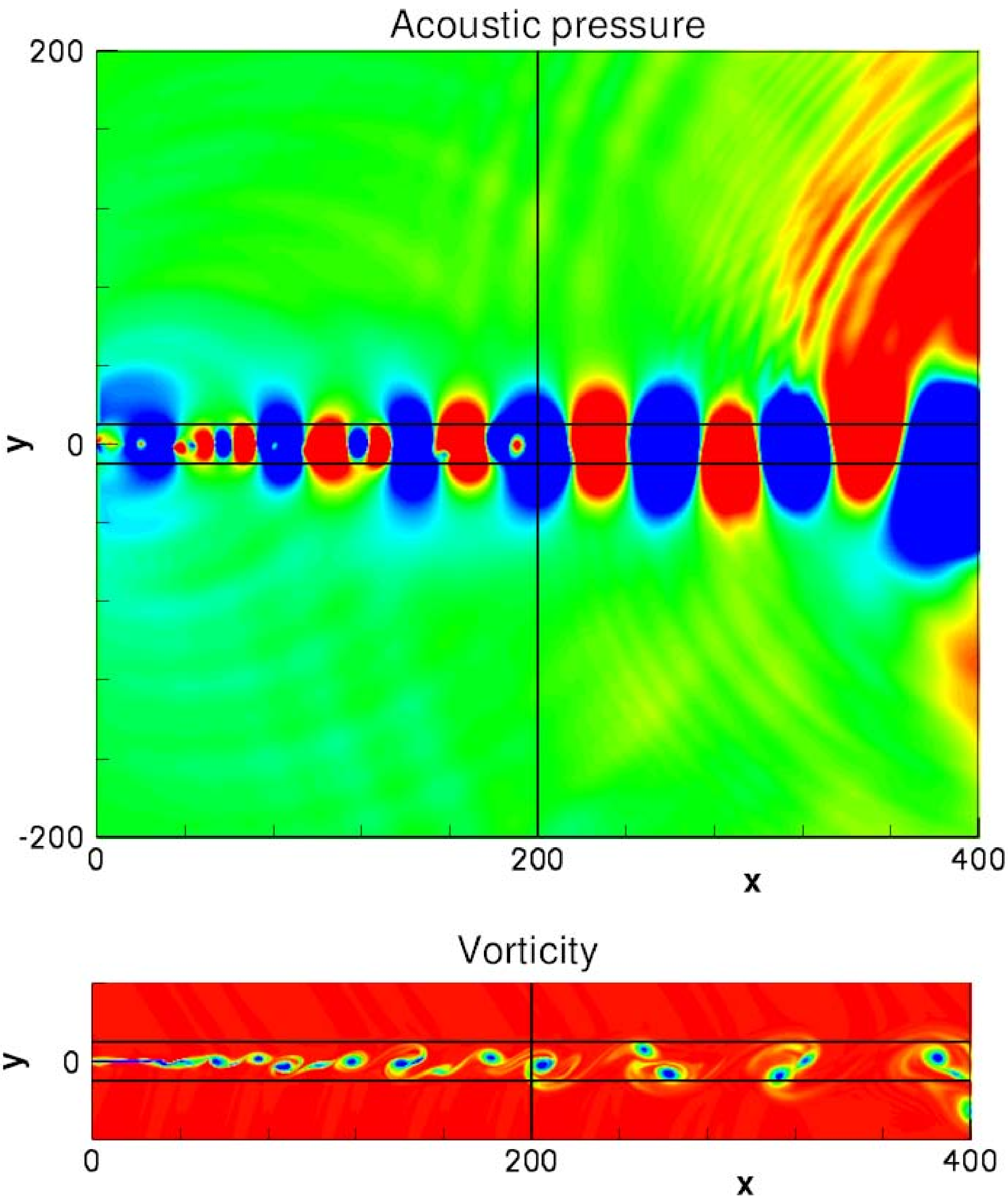


Figure 12: Results for the mixing layer test case with a CFD/CFD coupling: instantaneous acoustic pressure field (up) and vorticity (down).

The simulations are performed until time $t = 1200$, corresponding to about 30 periods of the fundamental frequency $f$. This time is probably too small to obtain a quasi-permanent state but is sufficient to establish the vortex roll up and pairings in the physical region under consideration. The resulting flow field is highly organized with three main vortex pairings located approximately at $x = 75$, $x = 150$ and $x = 250$. These vortex pairings act as sound sources of respectively frequency $f/2$, $f/4$ and $f/8$. The generated acoustic field is dominated by the interference of the waves emitted. Unfortunately, a strong mode appears at the downstream boundary and then overtakes progressively all the other modes. The apparent origin of this mode seems to be further in the sponge zone. Whether this mode is a spurious one or not is not clear and more investigations are needed to answer this. Other authors also seem to have experienced this (see for example [13]. In order to identify the first three aeroacoustic sources, authors generally cut their computational domain before $x = 300$ (see for example [23]).

Different computations have been run in order to investigate the potentiality and the limits of the proposed coupling methods. The first one concerns a CFD/CFD coupling in the near-field domains mesh with the same grid. Figure 12 shows instantaneous vorticity and acoustic pressure defined as $p_{acou} = (\gamma p - 1)1e + 5$. Non-dimensioned vorticity color scale is between 0 and 1.5 and pressure color scale is between -150 and 150 Pa. As the grids used in this computation are conformal in the x-direction, the results are supposed to be reference ones. In Figure 13, we can notice the good coupling between the different zones. Notice that, in this computation, the non-conforming Euler/Navier-Stokes coupling in the y-direction does not produce any spurious mode.

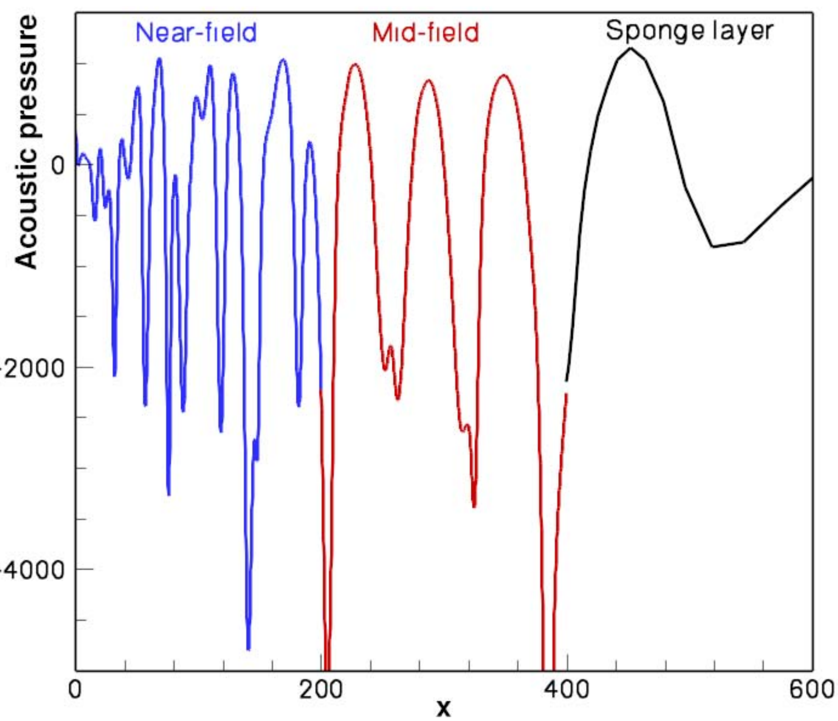


Figure 13: Instantaneous acoustic pressure distribution along the x-axis for the mixing layer test case with a CFD/CFD coupling.

Figure 14 shows the same fields for a CFD/CAA coupling. The CAA grid used in this computation has a grid meshing of 2, which emphasize the problems obtained with a grid meshing of 1. In Figure 15, we can notice visible discontinuity in pressure distribution between the different zones. Notice that, in this computation, spurious modes appear at the coupling coordinates $x = 200$ and $x = 400$.

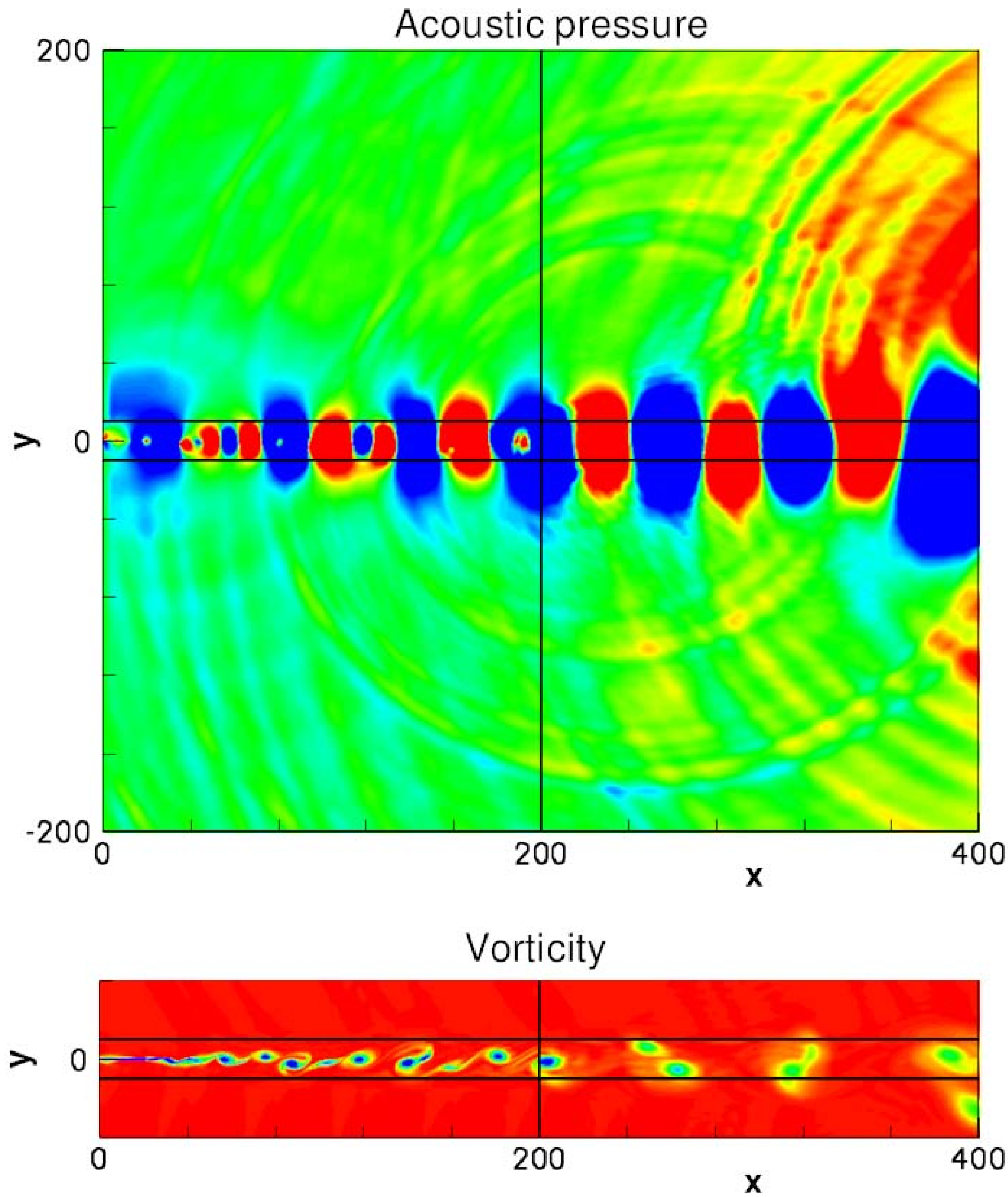


Figure 14: Results for the mixing layer test case with a CFD/CAA(dx=2) coupling: instantaneous acoustic pressure field (up) and vorticity (down).

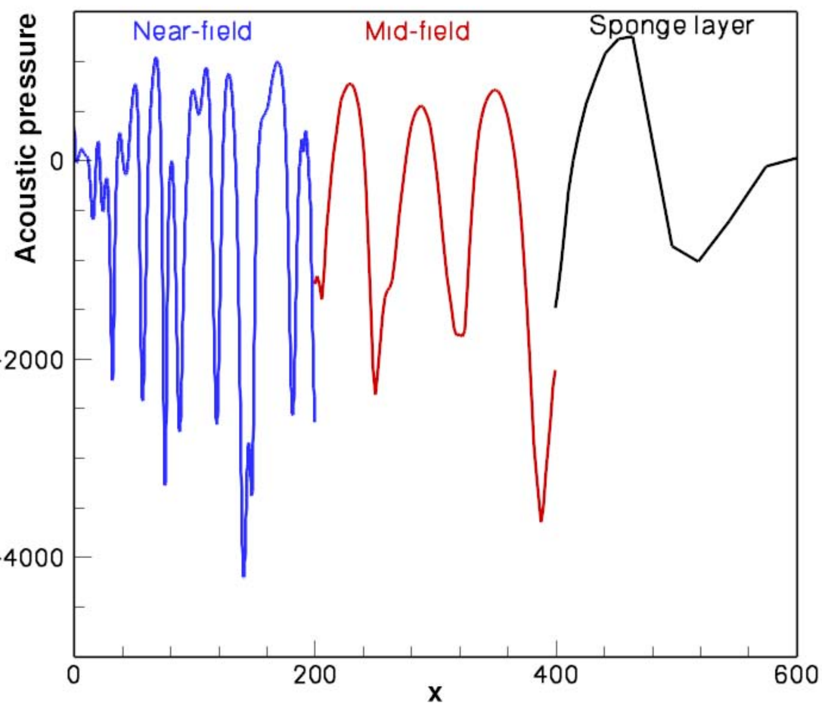


Figure 15: Instantaneous acoustic pressure distribution along the x-axis for the mixing layer test case with a CFD/CAA(dx=2) coupling.

# 6 Conclusion

An Euler/Navier-Stokes coupling akin to a chimera approach for multiscale aeroacoustic problems has been presented within the framework of DG. The EDG scheme which gives an accurate discretization of the viscous fluxes has been used for the Navier-Stokes computations.

In the EDG scheme, discontinuities are removed at each interface between elements by an $L^2$ projection on a staggered rectangular element whatever the shape elements is, called elastoplast. We generalized this technique to remove discontinuities, both in space and time, between computational domains due to non conformal grids. The EDG technique applied to the Euler/Navier-Stokes coupling is what makes the domain decomposition approach and the chimera approach similar.

The present study shows qualitative results of the possibility of the present approach. A qualitative comparison with an acoustic analogy prediction should be performed in the future to completely validate this approach. Nevertheless, first results presented on vortex shedding problems open the door to a new strategy for numerical acoustics with a strong coupling between CFD and CAA. Many points remain to be analysed such as more accurate outflow boundary conditions or improving the Schwarz algorithms.

This type of coupling has been numerically evaluated on the test case of the flow around a cylinder at low Reynolds number. As could be done for more complex applications, in 3D for example, we would use Cartesian grids for the acoustic simulations and unstructured meshes for the Navier-Stokes simulations, in particular near the cylinder. This first parallel result shows the interest of the domain decomposition technique in terms of computational cost versus a full Navier-Stokes computation. For very low Reynolds number, optimized transmission condition will have to be defined. For technical reasons, no results with the coupling in volume are available yet. Further work will consist in comparing the Chimera approach with the Schwarz relaxation technique on a detailed acoustic simulation.

Finally developments will include 3D simulations. For that purpose, the explicit time stepping of the Navier-Stokes solver will be replaced by an implicit one, as for example a space-time DG approach.

## References


[1] Borrel M., Halpern L. & Ryan J. *Euler/Navier-Stokes coupling for aeroacoustic problems*, Proceedings of the ICCFD6, Computational Fluid Dynamics 2010, Springer Ed.

[2] Borrel M., Halpern, L. & Ryan J. *Euler/Navier-Stokes couplings for multiscale aeroacoustic problems*, AIAA paper, 2011-3047.

[3] Borrel M. & Ryan J. *The Elastoplast Discontinuous Galerkin method (EDG) for the Navier-Stokes equations*, Journal of Comput. Physics, vol. 231, issue 1, pp. 1-22, 2012.

[4] Colonius, T. ,Lele S.K. & Moin, P. *Sound generation in a mixing layer*, J. Fluid Mech., pp. 375-409, 1997.

[5] Desquesnes, G. *Euler equations in perturbation 2.5-D: a new system for acoustic modal propagation*, AIAA paper 2008-2822.

[6] Lighthill, M.J. *Report on the final panel discussion on computational aeroacoustics*, ICASE Report 92-53, 1992.

[7] Marsden O., Bogey C. & Bailly C. *High-order curvilinear simulations of flows around non-Cartesian bodies*, Journal of Comput. Acoustics, Vol. 13, No. 4, pp 731-748, 2005.

[8] Toro E. F. , Spruce M., Speares W.: *Restoration of the contact surface in the HLL-Riemann solver*, Shock Waves 4, , 25ï¿¡34 (1994).

[9] Shu C.-W. & Osher S.: *Efficient implementation of essentially non-oscillatory shock-capturing schemes*, J. Comput. Phys. 77 , 439-471 (1988).

[10] Titarev V.A. & Toro E.F.: *ADER schemes for three-dimensional nonlinear hyperbolic systems*,Isaac Newton Institute for Mathematical Sciences Preprint Series, 2003.

[11] Schwarz H. A. *Über einen Grenzübergang durch alternierendes Verfahren.* Vierteljahrsschrift der Naturforschenden Gesellschaft in Zürich, 15, 272–286 (1870)

[12] Bennequin D., Gander M.J., Halpern L: *A homographic best approximation problem with application to optimized Schwarz waveform relaxation.* Math. Comp. 78, 185–223 (2009).

[13] Dumbser M.: *Arbitrary high order PNPM schemes on unstructured meshes for the compressible NavierŰStokes equations*, Computers & Fluids 39 (2010), 60-76.

[14] Marsden O., Bogey C. and Bailly C. : *High-order curvilinear simulations of flows around non-cartesian bodies*, Journal of Computational Acoustics, Vol. 13, No. 4 (2005) 731–748.

[15] Gander M.J., Halpern L., Japhet C. and Martin V: *Viscous Problems with Inviscid Approximations in Subregions: a New Approach Based on Operator Factorization*, ESAIM Proc 27, 272–288 (2009).

[16] Gassner G., Lörcher F. and Munz C.-D.: *A contribution to the construction of diffusion fluxes for finite volume and Discontinuous Galerkin schemes*, J. Comput. Phys., 224 (2007), pp. 1049-1064.

[17] Halpern L., Japhet C. and Szeftel J.: *Discontinuous Galerkin and nonconforming in time optimized Schwarz waveform relaxation*, proceedings of the Eighteenth International Conference on Domain Decomposition Methods, (http://numerik.mi.fu-berlin.de/DDM/DD18/) (2009).

[18] Lelarasmee E., Sangiovanni-Vincentelli A.L. and Ruehli A.E.: *The waveform relaxation method for time-domain analysis of large scale integrated circuits*, IEEE Trans. on Computer-Aided Design of Integrated Circuits and Systems, vol. CAD-1, 131–145 (1982).

[19] Lions P.-L.. *On the Schwarz alternating method. I.*: In Roland Glowinski, Gene H. Golub, Gérard A. Meurant, and Jacques Périaux, editors, *First International Symposium on Domain Decomposition Methods for Partial Differential Equations*, SIAM, 1–42 (1988).

[20] Geuzaine C., Remacle J.F.: *Gmsh: a three-dimensional finite element mesh generator with built-in pre- and post-processing facilities*, Int. J. for Num. Meth. in Eng. 79-11, 1309–1331 (2009).

[21] Utzmann J., F. LÍorcher F., M. Dumbser M. and C.ŰD. Munz C.-D.: *Aeroacoustic Simulations for Complex Geometries based on Hybrid Meshes*, AIAA paper 2006-2418, May 2005.

[22] Gassner G., Lörcher F. and Munz C.-D.: *A discontinuous Galerkin scheme based on a space-time expansion II. Viscous flow equations in multi dimension*, J. Sci. Comput., 34 (2007), pp. 260-286.

[23] Deneuve A., Druault P., Marchiano R. and Sagaut P.: *A coupled time-reversal/complex differentiation method for aeroacoustic sensitivity analysis: towards a source detection procedure*, J. Fluid Mech., 642 (2010), pp. 181-212.